

Article

Fenton-like Remediation for Industrial Oily Wastewater Using Fe₇₈Si₉B₁₃ Metallic Glasses

Yulong Liu ^{1,2} , Bowen Zhao ^{1,3,4}, Guofeng Ma ², Shiming Zhang ⁵, Haifeng Zhang ^{1,4} and Zhengwang Zhu ^{1,4,*} 

¹ Shi-Changxu Innovation Center for Advanced Materials, Institute of Metal Research, Chinese Academy of Sciences, Shenyang 110016, China

² College of Mechanical Engineering, Shenyang University, Shenyang 110044, China

³ School of Materials Science and Engineering, University of Science and Technology of China, Shenyang 110016, China

⁴ CAS Key Laboratory of Nuclear Materials and Safety Assessment, Institute of Metal Research, Chinese Academy of Sciences, Shenyang 110016, China

⁵ Qingdao Yunlu Advanced Materials Technology Co., Ltd., Qingdao 266232, China

* Correspondence: zzwzhu@imr.ac.cn

Abstract: Metallic glasses (MGs) with a unique atomic structure have been widely used in the catalytic degradation of organic pollutants in the recent years. Fe₇₈Si₉B₁₃ MGs exhibited excellent catalytic performance for the degradation of oily wastewater in a Fenton-like system for the first time. The oil removal and chemical oxygen demand (COD) removal from the oily wastewater were 72.67% and 70.18% within 60 min, respectively. Quenching experiments were performed to verify the production of active hydroxyl radicals ($\cdot\text{OH}$) by activating hydrogen peroxide (H₂O₂). The formation of $\cdot\text{OH}$ species can significantly contribute to the degradation reaction of oily wastewater. Fe₇₈Si₉B₁₃ MG ribbons were highly efficient materials that exhibited superior reactivity towards H₂O₂ activation in oily wastewater treatment. The study revealed the catalytic capability of metallic glasses, presenting extensive prospects of their applications in oily wastewater treatment.

Keywords: metallic glasses; oily wastewater; activation; catalytic degradation



Citation: Liu, Y.; Zhao, B.; Ma, G.; Zhang, S.; Zhang, H.; Zhu, Z. Fenton-like Remediation for Industrial Oily Wastewater Using Fe₇₈Si₉B₁₃ Metallic Glasses. *Catalysts* **2022**, *12*, 1038. <https://doi.org/10.3390/catal12091038>

Academic Editors: Gassan Hodaifa, Rafael Borja and Mha Albqmi

Received: 10 August 2022

Accepted: 5 September 2022

Published: 12 September 2022

Publisher's Note: MDPI stays neutral with regard to jurisdictional claims in published maps and institutional affiliations.



Copyright: © 2022 by the authors. Licensee MDPI, Basel, Switzerland. This article is an open access article distributed under the terms and conditions of the Creative Commons Attribution (CC BY) license (<https://creativecommons.org/licenses/by/4.0/>).

1. Introduction

Waste sludge containing large amounts of mineral oil is produced in the metal manufacturing process, which is classified as a high concentration hazardous waste [1–3]. About 10–20 tons of oily wastewater will be produced from cleaning 1 ton of waste sludge. This leads to a huge discharge of oily wastewater. The organic pollutants in oily wastewater have certain characteristics, such as high concentration, complex composition, biological toxicity and refractory [4–7]. At present, a large number of advanced treatment technologies for oily wastewater are systematically implemented [8–11]. Compared to conventional techniques, advanced oxidation processes (AOPs) have been extensively studied as a promising technique due to their superior degradation and mineralization efficiency of pollutants in wastewater [12,13]. Very recently, owing to the advantage of abundant natural resources, low cost and environmental friendliness, Fe-based catalytic materials have been extensively used for the degradation of organic contaminants in AOPs system. However, the catalysts like magnetite (Fe₃O₄) [14] and zero valent iron (ZVI) [15] still have certain disadvantages, such as low efficiency, poor reusability, fast decay and secondary pollution [16]. To overcome the aforementioned limitations, Fe-based MGs are utilized, which could effectively enhance the catalytic activity by improving the internal atomic arrangement [17] and tuning the chemical composition [18,19].

Metallic glasses with short range ordered and long range disordered atomic structure were usually employed as structural materials for different industrial applications due to improved mechanical properties, soft ferromagnetism and corrosion resistance [20–22].

Additionally, a great number of studies have been showed that the metallic glasses with various alloy systems exhibited superior catalytic degradation behaviors of organic pollutants owing to high reactivity [23–25]. For instance, the $\text{Cu}_{46}\text{Zr}_{42}\text{Al}_7\text{Y}_5$ MG ribbons showed excellent catalytic performance for acid orange II degradation with a degradation efficiency of 96.05% and a COD removal of 51.73% [26]. A maximum degradation efficiency of 98% for congo red is achieved using $\text{Mg}_{60}\text{Zn}_{35}\text{Ca}_5$ MG powders [27]. Moreover, the direct blue 2B solutions can be completely degraded by Al-based MG ribbons under wide pH conditions [19]. Similarly, the unexpected organic pollutant degradation performance of Fe-based MGs was revealed. Amorphous $\text{Fe}_{84}\text{B}_{16}$ exhibited degradation of direct blue 6 dye 1.8 and 89 times faster compared to the Fe-B crystalline alloy and commercial iron powder, respectively [28]. Furthermore, $\text{Fe}_{78}\text{Si}_9\text{B}_{13}$ MGs exhibited excellent production rate of active radical species among various Fe-based catalysts [29]. As a result, $\text{Fe}_{78}\text{Si}_9\text{B}_{13}$ MGs have been widely used for wastewater treatment [30–32], providing an environmentally functional material for the catalytic degradation of organic contaminants.

In this work, oily wastewater degradation and mineralization were investigated using $\text{Fe}_{78}\text{Si}_9\text{B}_{13}$ MGs. These catalytic materials serve as an alternative Fe^{2+} releasing source that can produce $\cdot\text{OH}$ radicals by activating H_2O_2 (Fenton-like system). $\text{Fe}_{78}\text{Si}_9\text{B}_{13}$ MGs were found to be highly efficient catalysts that showed improved degradation performance of oily wastewater in terms of oil removal and COD removal. Moreover, the stability and durability of $\text{Fe}_{78}\text{Si}_9\text{B}_{13}$ MGs were discussed based on recycling experiments. The catalytic mechanism was proposed based on the structural and morphological variations of catalysts combined with free radical quenching experiments.

2. Materials and Methods

2.1. Materials

The alloy ingots with nominal composition of $\text{Fe}_{78}\text{Si}_9\text{B}_{13}$ were prepared by arc melting of a mixture of Fe, Si and B with greater purity than 99.9 wt% under a Ti-gettered Ar atmosphere. The master alloy ingot was melted by induction heating in a quartz crucible. The molten master alloy ingot was ejected onto a chilled copper roll surface to prepare the as-melt MG ribbons of $\text{Fe}_{78}\text{Si}_9\text{B}_{13}$. The waste oily sludge was supplied by Shenyang General Magnetic Co., Ltd., Shenyang, China. The oily wastewater was prepared by stirring for 30 min and centrifuging sludge mixtures with an oil–water ratio of 1:20, 1:40, 1:60 and 1:80 (wt%).

2.2. Characterization

The structural features of the as-melt and reacted $\text{Fe}_{78}\text{Si}_9\text{B}_{13}$ ribbons were characterized by X-ray diffraction (XRD, Rigaku D/max-2500PC, Tokyo, Japan) with $\text{Co-K}\alpha$ radiation. The surface morphologies of the ribbons before and after the catalytic organic pollutant degradation were characterized using a scanning electron microscope (SEM, Zeiss SUPPA 55, Oberkochen, Germany). The crystallization behavior of the melt and reacted ribbons was characterized by differential scanning calorimetry (Netzsch DSC 404C, Selbu, Germany).

2.3. Analytical Methods

All oily wastewater removal experiments were conducted in a 250 mL glass beaker with a stirring speed of 300 rpm by a mechanical stirrer (Changzhou Jaboson Instrument JJ-1, Changzhou, China). The oily wastewater of 200 mL in a glass beaker was placed in a thermostat water bath at the desired temperature. The solution pH values were adjusted by diluted HCl solution ($1 \text{ mol}\cdot\text{L}^{-1}$) and diluted NaOH ($0.1 \text{ mol}\cdot\text{L}^{-1}$). At every 10 min interval, about 10 mL aliquot of the reaction mixture was collected and centrifuged. The supernatant liquid was tested by infrared spectrophotometer (Tianjin Tianguang TJ270-30A, Tianjin, China) and chemical oxygen demand detector (COD, Beijing Lianhua 5B-3(B), Beijing, China). The ion concentration of the oily wastewater samples before and after the reactions was measured by inductively coupled plasma-optical emission spectrometer (ICP-OES 720, Agilent Technologies Inc., Palo Alto, America). The active radical species were analyzed

using an electron paramagnetic resonance spectrometer (EPR, Bruker A300, Karlsruhe, Germany) with 5,5-dimethyl-1-pyrroline N-oxide (DMPO) as the spin-trapping agent.

3. Results and Discussion

3.1. Catalytic Capability

3.1.1. Effect of pH Value

Figure 1a shows the effect of pH value (from 2 to 7) on oil removal. It is observed that the oil removal sharply reduces with increasing of pH value. Oil removal of 72.67% can be achieved within 60 min at pH = 3. In contrast, only 52.14% oil removal was observed at pH = 7. The enhanced degradation performance at lower pH value may be due to the influence of pH on stability of H₂O₂ [33,34]. As shown in Figure 1b, the COD removal of 70.18% was achieved within 60 min at pH = 3, indicating the favorable mineralization efficiency of oily wastewater. Under a high pH system, some side effects lead to reducing the degradation capability due to formation of sediment, following Equations (1) and (2) [35,36].

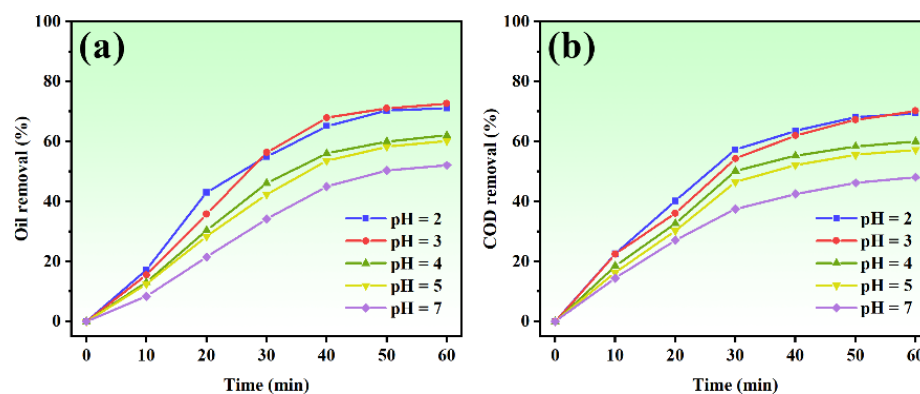
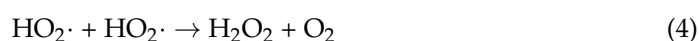


Figure 1. Effect of pH value on (a) oil removal and (b) COD removal. (H₂O₂ concentration: 0.12 mol·L⁻¹, catalyst dosage: 1.5 g·L⁻¹, oil–water mass ratio: 1:60, temperature: 40 °C).

3.1.2. Effect of H₂O₂ Concentration

As shown in Figure 2a, the oil removal is 55.10% when the H₂O₂ concentration is 0.08 mol·L⁻¹. Apparently, the oil removal increased to 63.34% and 70.97% within 60 min at H₂O₂ concentrations of 0.10 and 0.14 mol·L⁻¹, respectively. As the H₂O₂ concentration increased further to 0.16 mol·L⁻¹, the oil removal decreased. COD removal displayed the similar results as shown in Figure 2b. The degradation capability of COD removal increases and then decreases with H₂O₂ concentration. The reason may be that the quantity of ·OH radicals play a significant role in the oily wastewater degradation [37,38]. Moreover, the excessive H₂O₂ concentration results in ·OH radicals self-quenching to form the weak oxidizing hydroperoxy radicals (·O₂H radicals) via Equations (3) and (4).



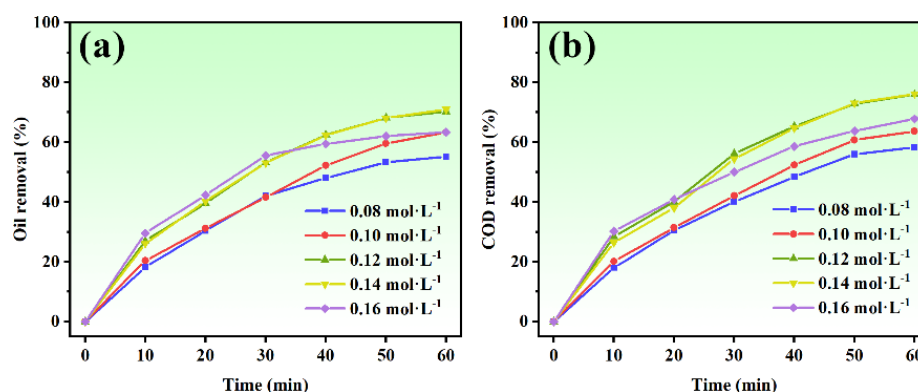


Figure 2. Effect of H₂O₂ concentration on (a) oil removal and (b) COD removal. (pH = 3, catalyst dosage: 1.5 g·L⁻¹, oil–water mass ratio: 1:60, temperature: 40 °C).

3.1.3. Effect of Catalyst Dosage

As seen from Figure 3a, the oil removal significantly enhanced from 53.35% to 72.23% within 60 min when the catalyst dosage increased from 0.5 g·L⁻¹ to 1.5 g·L⁻¹. The oil removal slightly increased with a further increase in catalyst loading to 2.0 g·L⁻¹. COD removal increased with an increase in the catalyst loading as shown in Figure 3b. When the MG ribbon dosage is 2.0 g·L⁻¹, the COD removal stabilized at around 72%. Normally, the organic molecule decomposition takes place via direct surface reaction on active iron species [39]. Increasing the amount of catalyst provides more active sites, thereby achieving faster production rate of ·OH radical species. However, excessive addition of catalyst would provide more Fe³⁺, which would work against catalytic efficiency [40,41].

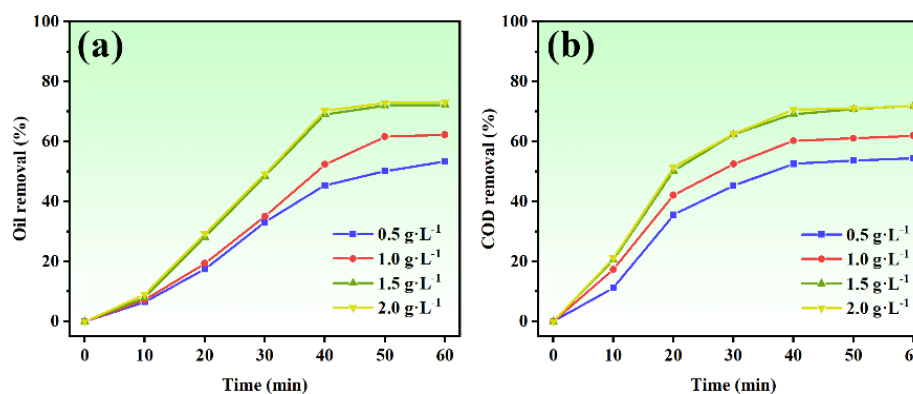


Figure 3. Effect of catalyst dosage on (a) oil removal and (b) COD removal. (H₂O₂ concentration: 0.12 mol·L⁻¹, pH = 3, oil–water mass ratio: 1:60, temperature: 40 °C).

3.1.4. Effect of Oil–Water Mass Ratio

As the oil–water mass ratio increases, the initial oil concentration increases. As seen in Figure 4a, the faster oil removal is observed for the lower the oil–water mass ratio in the first 10 min of reaction. Figure 4b shows the effect of the oil–water mass ratio on COD removal with an oil to water in the ratio (by mass) 1:80 to 1:20. With the increase of the oil–water mass ratio, the COD removal is obviously reduced. This is because more organic molecules exist in the system of larger oil–water mass ratio as the reaction progresses, thereby leading to the weak degradation behaviors in the presence of the same amount of ·OH radicals.

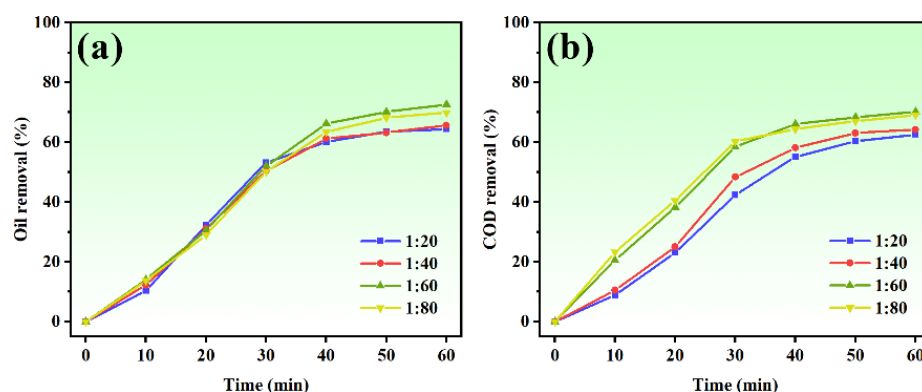


Figure 4. Effect of oil–water mass ratio on (a) oil removal and (b) COD removal (H_2O_2 concentration: $0.12 \text{ mol}\cdot\text{L}^{-1}$, $\text{pH} = 3$, catalyst dosage: $1.5 \text{ g}\cdot\text{L}^{-1}$, temperature: $40 \text{ }^\circ\text{C}$).

3.1.5. Effect of Reaction Temperature

Regarding chemical reactions, the reaction temperature can be always considered as an important experimental parameter. According to the principle of reaction kinetics, the molecules colliding with each other in solution will be accelerated and energized with the increase of reaction temperature, thus speeding up the reaction. The evaluation of the degradation behaviors in temperature ranging from 25 to $45 \text{ }^\circ\text{C}$ as shown in Figure 5a,b. The oil removal and COD removal remarkably increase along with the increase of reaction temperature. When the temperature increases to $45 \text{ }^\circ\text{C}$, the degradation behavior is not significantly improved.

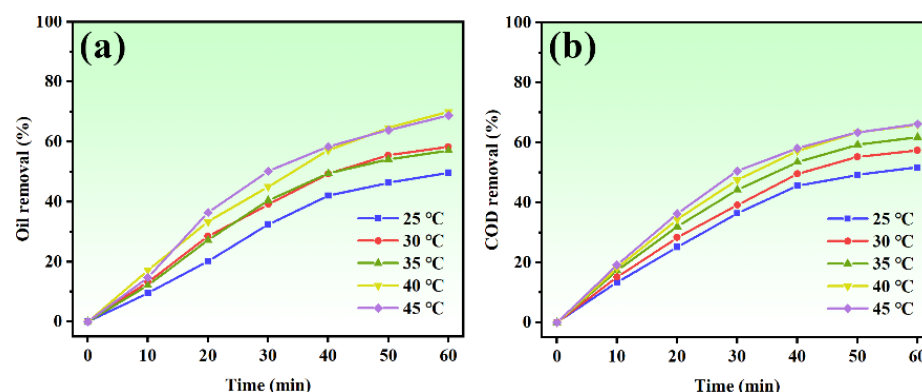


Figure 5. Effect of reaction temperature on (a) oil removal and (b) COD removal. (H_2O_2 concentration: $0.12 \text{ mol}\cdot\text{L}^{-1}$, $\text{pH} = 3$, catalyst dosage: $1.5 \text{ g}\cdot\text{L}^{-1}$, oil–water mass ratio: 1:60).

3.1.6. Stability and Reusability

The stability and reusability of metallic glassy catalysts are the extremely important capabilities for degradation of organic pollutants [42]. Figure 6 shows the catalytic reusability using $\text{Fe}_{78}\text{Si}_9\text{B}_{13}$ MGs from the 1st to 3rd run for degrading oily wastewater. Clearly, the COD removal still maintains as high as 68% after 60 min for three cycles, suggesting the excellent reuse life. Notably, the COD removal for the 2nd run is little better than that for the 1st run due to surface activation. The slight decay is observed on the ribbon surface after the 2nd run, forming SiO_2 layers during the degradation of oily wastewater [8]. Abundant Fe^{2+} irons can be supplied by falling the oxide layers for activating H_2O_2 , thereby further improving the catalytic reusability [43,44]. For the 3rd run, the COD removal slightly decreases due to the side effect of oxide deposition.

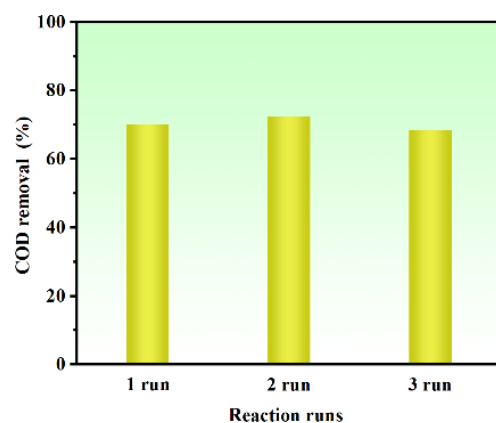


Figure 6. Reaction runs for oily wastewater removal by $\text{Fe}_{78}\text{Si}_9\text{B}_{13}/\text{H}_2\text{O}_2$ system (H_2O_2 concentration: $0.12 \text{ mol}\cdot\text{L}^{-1}$, $\text{pH} = 3$, catalyst dosage: $1.5 \text{ g}\cdot\text{L}^{-1}$, oil–water mass ratio: 1:60, temperature: $40 \text{ }^\circ\text{C}$).

3.2. Structures and Surface Morphology

In order to further investigate stability, the structures and surface morphology of the ribbons were characterized, respectively. Figure 7a displays the XRD patterns of the as-received and reused 3rd $\text{Fe}_{78}\text{Si}_9\text{B}_{13}$ metallic glass ribbons. The XRD patterns of as-received and reused ribbons present a broad diffraction peak at $2\theta = 40\sim 50^\circ$, indicating that all the ribbons are mainly in the amorphous state [45]. However, the 3rd run recycled $\text{Fe}_{78}\text{Si}_9\text{B}_{13}$ metallic glass ribbons have a crystallization peak, indicating crystalline precipitated phase of $\alpha\text{-Fe}$ on the surface of the ribbons [46,47]. As shown in Figure 7b, each of DSC curves clearly displays the exothermic peak, further obtaining thermodynamic parameters of T_{p1} and T_{p2} . The amorphous nature was also verified by DSC measurements. According to the existence of two exothermic peaks in DSC curves and the intensity of T_{p1} and T_{p2} is raised, the crystallization process can be roughly divided into two steps: one is the precipitation process of primary $\alpha\text{-Fe}$ phase and the other is the precipitation process of boride [48]. According to the Dubois model [49], Fe-Si-B series alloys are composed of Fe-B and Fe-Si regions. The precipitation of $\alpha\text{-Fe}$ may accelerate the decomposition of Fe-B region due to heteronucleation [50].

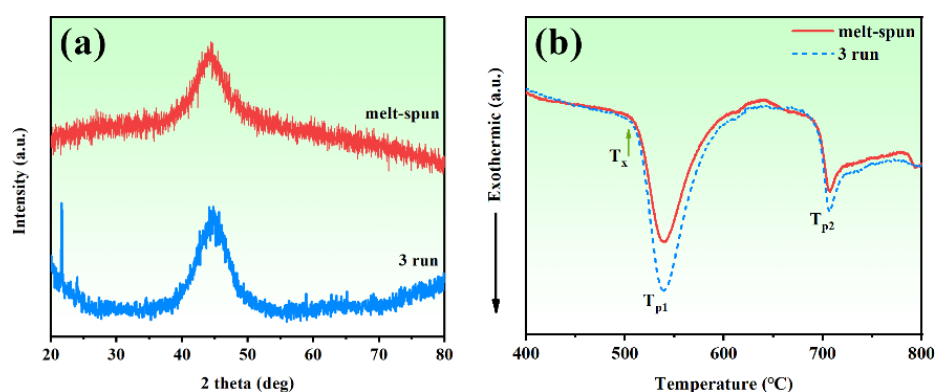


Figure 7. (a) XRD patterns and (b) DSC curves of the melt-spun and 3rd reused $\text{Fe}_{78}\text{Si}_9\text{B}_{13}$ metallic glass ribbons.

Figure 8 shows the SEM images of the melt-spun, 1st and 3rd reused $\text{Fe}_{78}\text{Si}_9\text{B}_{13}$ ribbons. It can be observed that the surface morphology of melt-spun ribbons is very smooth without obvious surface defects as shown in Figure 8a. Although the surface of the ribbons presents a slight decay with several corrosion areas in Figure 8b, most of the surface remains relative smooth. As seen from Figure 8c, some corrosion products are precipitated and accumulated on the surface of the ribbons for area B, except for the small

regions of smooth surface for area A. These products are covered with active substances, further leading to the reduction of catalytic degradation reaction.

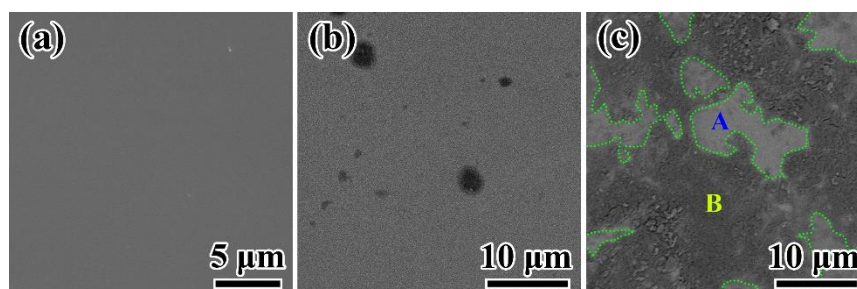


Figure 8. SEM images of the (a) as-received, (b) 1st and (c) 3rd reused $\text{Fe}_{78}\text{Si}_9\text{B}_{13}$ metallic glass ribbons.

3.3. Reaction Mechanism

It has been recognized that the mechanism for degradation of organic contaminants is attributed to the catalytic oxidation of activated $\cdot\text{OH}$ radicals in the Fenton process. The *o*-Phenylenediamine (OPDA) as typical catcher of $\cdot\text{OH}$ radicals was used to verify the catalytic contribution of $\cdot\text{OH}$ radicals. The OPDA will react with $\cdot\text{OH}$ radicals to form 2,3-diaminophenazine (DAPN) stabilizing in solution for a long time. Figure 9a shows the effect of OPDA concentration on COD removal from 0 to 20 $\text{mmol}\cdot\text{L}^{-1}$. It is observed that the COD removal sharply decreases with increasing of OPDA concentration. Meanwhile, the reaction rate rapidly decreases in Figure 9b. The reason may be that the active $\cdot\text{OH}$ radicals preferentially combine with OPDA to produce DAPN rather than degrading organic pollutants.

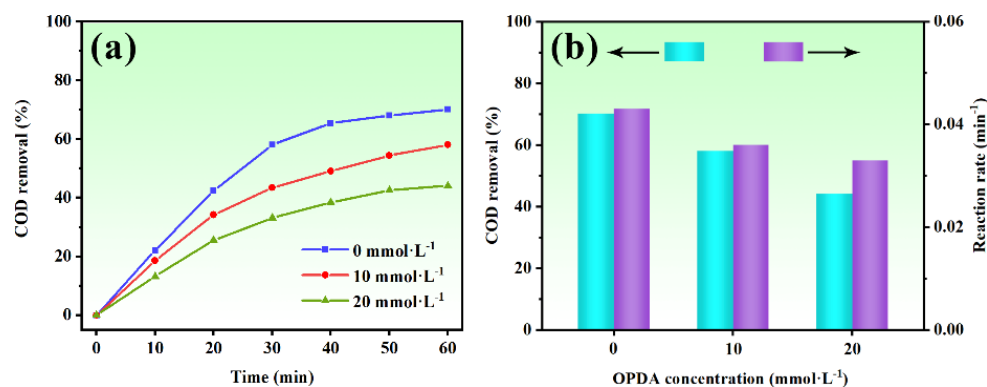


Figure 9. Effect of OPDA concentration on (a) the normalized as a function of reaction time, (b) COD removal and reaction rate. (H_2O_2 concentration: $0.12\text{ mol}\cdot\text{L}^{-1}$, pH = 3, catalyst dosage: $1.5\text{ g}\cdot\text{L}^{-1}$, oil–water mass ratio: 1:60, temperature: $40\text{ }^\circ\text{C}$).

The active radical species were observed by EPR technique with DMPO as spin-trapping agent. As shown in Figure 10, variation for aliquots of samples collected at 10 min and 20 min of reaction interval in intensity of $\cdot\text{OH}$ radicals is obvious between 3480 and 3540 of magnetic field. The relative intensity of $\cdot\text{OH}$ radicals increased with the prolongation of reaction time. To combine with the above results, $\cdot\text{OH}$ radicals play an important role in the whole Fenton-like degradation process of oily wastewater.

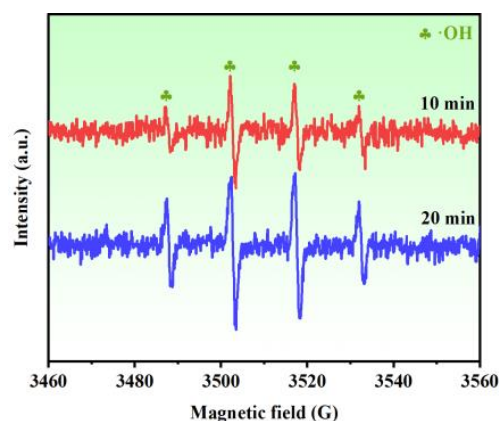


Figure 10. Intensity of ·OH radicals in oily wastewater during the Fenton-like process.

Various ion concentrations of solution system before and after the reactions are analyzed in Table 1. The variation on majority of ions concentration is slight, whereas iron ions in solution have a great increased. A mass of Fe^{2+} and Fe^{3+} flow into the solution because of corrosion action and Fe^0 plays an important role is confirmed at the same time. Furthermore, Figure 11 shows the forming process of ·OH radicals in the Fenton reaction. It is well known that Fe^{2+} acts as the main active source to activate H_2O_2 producing active species for ·OH radicals (Equation (5)) [16]. However, the formation of Fe^{2+} is more likely by direct reaction between zero-valent iron in the $\text{Fe}_{78}\text{Si}_9\text{B}_{13}$ ribbons and a small amount of H_2O_2 molecules (Equation (6)) [23]. In addition, the electrons of amorphous Fe atom on $4s^2$ orbital are extraordinarily unstable and active, thereby leading to forming Fe^{2+} by losing electrons (Equation (7)) [11]. Besides this, there are reciprocal transitions between the iron ions for the Fe^{2+} and Fe^{3+} under certain conditions as the reaction continues (Equations (8)–(10)). According to the continuous reaction process, the Fe^{2+} will react with H_2O_2 to produce moderate activated ·OH radicals, contributing to enhancing the catalytic degradation reaction [9]. Therefore, the major reaction equations are as the following Equations (5)–(10):

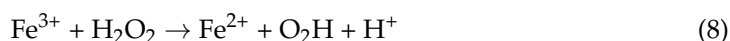
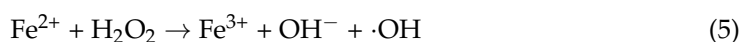


Table 1. Comparative variations of ion concentration before and after the reaction.

Ion	Ion Concentration ($\text{mg}\cdot\text{L}^{-1}$)	
	Before Reaction	After Reaction
Li^+	<0.2	<0.2
K^+	6.4	8.1
Mg^+	5.4	7.1
$\text{Fe}^{2+}/\text{Fe}^{3+}$	2.5	251.3
Ca^{2+}	29.9	40.3
Si^{4+}	4.0	10.7
B^{3+}	5.8	11.7

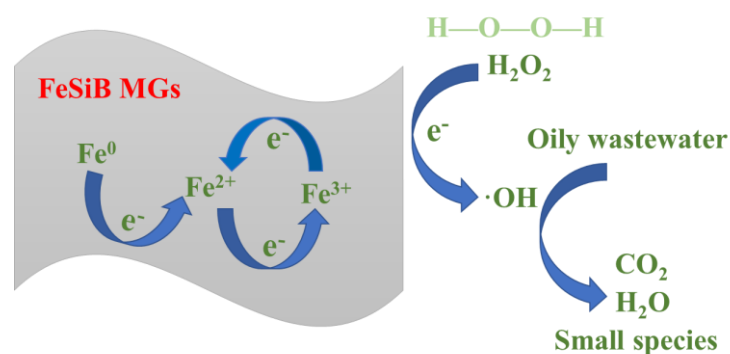


Figure 11. Schematic illustration for the Fenton-like degradation of oily wastewater using Fe₇₈Si₉B₁₃ metallic glassy ribbons.

4. Conclusions

In this work, the Fe₇₈Si₉B₁₃ MGs as efficient catalysts demonstrate excellent catalytic degradation behavior towards oily wastewater treatment in H₂O₂ activation system. The conclusions are as follows:

- (1) The oil removal and COD removal of oily wastewater are achieved as high as 72.67% and 70.18% within 60 min using Fe₇₈Si₉B₁₃ MG ribbons under the optimum conditions, respectively.
- (2) The Fe₇₈Si₉B₁₃ MGs present the superior stability and reusability for 3 times with high COD removal during oily wastewater degradation.
- (3) The enhanced degradation performance may be mainly attributed to activate H₂O₂ molecules to generate ·OH radicals in the EPR analysis and quenching experiments. The Fe₇₈Si₉B₁₃ MGs provide a potential strategy for activating abundant ·OH radicals during oily wastewater degradation.

Author Contributions: Conceptualization, Y.L. and Z.Z.; methodology, B.Z. and Z.Z.; validation, Y.L., B.Z. and Z.Z.; writing—original draft preparation, Y.L.; writing—review and editing, Y.L., B.Z., G.M., S.Z., H.Z. and Z.Z.; supervision, G.M. and Z.Z.; funding acquisition, H.Z. and Z.Z.; All authors have read and agreed to the published version of the manuscript.

Funding: The work was supported by the National Natural Science Foundation of China (51801209 and 52074257), the Fund of Qingdao (19-9-2-1-wz).

Data Availability Statement: All relevant data are included in the paper.

Conflicts of Interest: The authors declare no conflict of interest.

References

1. Zhang, B.; Huang, K.; Wang, Q.; Li, G.; Wu, T.; Li, Y. Highly efficient treatment of oily wastewater using magnetic carbon nanotubes/layered double hydroxides composites. *Colloids Surf. A* **2020**, *586*, 124187. [[CrossRef](#)]
2. Khalifa, O.; Banat, F.; Srinivasakannan, C.; AlMarzooqi, F.; Hasan, S.W. Ozonation-assisted electro-membrane hybrid reactor for oily wastewater treatment: A methodological approach and synergy effects. *J. Clean. Prod.* **2021**, *289*, 125764. [[CrossRef](#)]
3. Zhong, L.; Sun, C.; Yang, F.; Dong, Y. Superhydrophilic spinel ceramic membranes for oily emulsion wastewater treatment. *J. Water Process Eng.* **2021**, *42*, 102161. [[CrossRef](#)]
4. Ahmad, T.; Guria, C.; Mandal, A. A review of oily wastewater treatment using ultrafiltration membrane: A parametric study to enhance the membrane performance. *J. Water Process Eng.* **2020**, *36*, 101289. [[CrossRef](#)]
5. Behroozi, A.H.; Ataabadi, M.R. Improvement in microfiltration process of oily wastewater: A comprehensive review over two decades. *J. Environ. Chem. Eng.* **2020**, *9*, 104981. [[CrossRef](#)]
6. Zhao, C.L.; Zhou, J.Y.; Yan, Y.; Yang, L.W.; Xing, G.H.; Li, H.Y.; Wu, P.; Wang, M.Y.; Zheng, H.L. Application of coagulation/flocculation in oily wastewater treatment: A review. *Sci. Total Environ.* **2021**, *765*, 142795. [[CrossRef](#)]
7. Liang, H.; Esmaeili, H. Application of nanomaterials for demulsification of oily wastewater: A review study. *Environ. Technol. Innov.* **2021**, *22*, 101498. [[CrossRef](#)]
8. Ikhsan, S.N.W.; Yusof, N.; Aziz, F.; Ismail, A.F.; Jaafar, J.; Salleh, W.N.W.; Misdan, N. Superwetting materials for hydrophilic-oleophobic membrane in oily wastewater treatment. *J. Environ. Manag.* **2021**, *290*, 112565. [[CrossRef](#)]

9. Ismail, N.H.; Salleh, W.N.W.; Ismail, A.F.; Hasbullah, H.; Yusof, N.; Aziz, F.; Jaafar, J. Hydrophilic polymer-based membrane for oily wastewater treatment: A review. *Sep. Purif. Technol.* **2020**, *233*, 116007. [[CrossRef](#)]
10. Liu, C.H.; Xia, J.Y.; Gu, J.C.; Wang, W.Q.; Liu, Q.Q.; Yan, L.K.; Chen, T. Multifunctional CNTs-PAA/MIL101(Fe)@P composite membrane for high-throughput oily wastewater remediation. *J. Hazard. Mater.* **2021**, *403*, 123547. [[CrossRef](#)]
11. Yaacob, N.; Sean, G.P.; Nazri, N.A.M.; Ismail, A.F.; Abidin, M.N.Z.; Subramaniam, M.N. Simultaneous oily wastewater adsorption and photodegradation by ZrO₂-TiO₂ heterojunction photocatalysts. *J. Water Process Eng.* **2021**, *39*, 101644. [[CrossRef](#)]
12. Jia, Z.; Liang, S.X.; Zhang, W.C.; Wang, W.M.; Yang, C.; Zhang, L.C. Heterogeneous photo Fenton-like degradation of the cibacron brilliant red 3B-A dye using amorphous Fe₇₈Si₉B₁₃ and Fe_{73.5}Si_{13.5}B₉Cu₁Nb₃ alloys: The influence of adsorption. *J. Taiwan Inst. Chem. Eng.* **2017**, *71*, 128–136. [[CrossRef](#)]
13. Jia, Z.; Miao, J.; Lu, H.; Habibi, D.; Zhang, W. Photocatalytic degradation and absorption kinetics of cibacron brilliant yellow 3G-P by nanosized ZnO catalyst under simulated solar light. *J. Taiwan Inst. Chem. Eng.* **2015**, *60*, 267–274. [[CrossRef](#)]
14. Usman, M.; Faure, P.; Hanna, K.; Abdelmoula, M.; Ruby, C. Application of magnetite catalyzed chemical oxidation (Fenton-like and persulfate) for the remediation of oil hydrocarbon contamination. *Fuel* **2012**, *96*, 270–276. [[CrossRef](#)]
15. Grčić, I.; Papić, S.; Žižek, K.; Koprivanac, N. Zero-valent iron (ZVI) Fenton oxidation of reactive dye wastewater under UV-C and solar irradiation. *Chem. Eng. J.* **2012**, *195*, 77–90. [[CrossRef](#)]
16. Jia, Z.; Zhang, W.; Wang, W.; Habibi, D. Amorphous Fe₇₈Si₉B₁₃ alloy: An efficient and reusable photo-enhanced Fenton-like catalyst in degradation of cibacron brilliant red 3B-A dye under UV-vis light. *Appl. Catal. B Environ.* **2016**, *192*, 46–56. [[CrossRef](#)]
17. Song, D.S.; Kim, J.H.; Fleury, E.; Kim, W.T.; Kim, D.H. Synthesis of ferromagnetic Fe-based bulk glassy alloys in the Fe-Nb-B-Y system. *J. Alloys Compd.* **2005**, *389*, 159–164. [[CrossRef](#)]
18. Liu, P.; Zhang, J.L.; Zha, M.Q.; Shek, C.H. Synthesis of an Fe Rich Amorphous Structure with a Catalytic Effect to Rapidly Decolorize Azo Dye at Room Temperature. *ACS Appl. Mater. Interfaces* **2014**, *6*, 5500–5505. [[CrossRef](#)]
19. Wang, P.; Wang, J.-Q.; Li, H.; Yang, H.; Huo, J.; Wang, J.; Chang, C.; Wang, X.; Li, R.-W.; Wang, G. Fast decolorization of azo dyes in both alkaline and acidic solutions by Al-based metallic glasses. *J. Alloys Compd.* **2017**, *701*, 759–767. [[CrossRef](#)]
20. Wang, W.H. Bulk metallic glasses with functional physical properties. *Adv. Mater.* **2009**, *21*, 4524–4544. [[CrossRef](#)]
21. Li, H.; Pang, S.; Liu, Y.; Sun, L.; Liaw, P.K.; Zhang, T. Biodegradable Mg–Zn–Ca–Sr bulk metallic glasses with enhanced corrosion performance for biomedical applications. *Mater. Des.* **2015**, *67*, 9–19. [[CrossRef](#)]
22. Baron-Wiechec, A.; Szewieczek, D.; Nawrat, G. Corrosion of amorphous and nanocrystalline Fe-based alloys and its influence on their magnetic behavior. *Electrochim. Acta* **2007**, *52*, 5690–5695. [[CrossRef](#)]
23. Wang, X.; Pan, Y.; Zhu, Z.; Wu, J. Efficient degradation of rhodamine B using Fe-based metallic glass catalyst by Fenton-like process. *Chemosphere* **2014**, *117*, 638–643. [[CrossRef](#)]
24. Zhao, B.W.; Zhu, Z.W.; Qin, X.D.; Li, Z.K.; Zhang, H.F. Highly efficient and stable CuZr-based metallic glassy catalysts for azo dye degradation. *J. Mater. Sci. Technol.* **2020**, *46*, 88–97. [[CrossRef](#)]
25. Wang, J.Q.; Liu, Y.H.; Chen, M.W.; Luzgin, D.V.L.; Inoue, A.; Perepezko, J.H. Excellent capability in degrading azo dyes by MgZn-based metallic glass powders. *Sci. Rep.* **2012**, *2*, 418. [[CrossRef](#)]
26. Yang, X.; Xu, X.C.; Xiang, Q.C.; Qu, Y.D.; Ren, Y.L.; Qiu, K.Q. The catalytic performance of Cu₄₆Zr_{47-x}Al₇Y_x amorphous ribbons in the degradation of AOII dye wastewater. *Environ. Sci. Pollut. R.* **2021**, *28*, 48038–48052. [[CrossRef](#)]
27. Ramya, M.; Karthika, M.; Selvakumar, R.; Raj, B.; Ravi, K. A facile and efficient single step ball milling process for synthesis of partially amorphous Mg–Zn–Ca alloy powders for dye degradation. *J. Alloys Compd.* **2017**, *696*, 185–192. [[CrossRef](#)]
28. Tang, Y.; Shao, Y.; Chen, N.; Yao, K.-F. Rapid decomposition of Direct Blue 6 in neutral solution by Fe–B amorphous alloys. *RSC Adv.* **2015**, *5*, 6215–6221. [[CrossRef](#)]
29. Jia, Z.; Kang, J.; Zhang, W.C.; Wang, W.M.; Yang, C.; Sun, H.; Habibi, D.; Zhang, L.C. Surface aging behavior of Fe-based amorphous alloys as catalysts during heterogeneous photo Fenton-like process for water treatment. *Appl. Catal. B Environ.* **2017**, *204*, 537–547. [[CrossRef](#)]
30. Ghorbani, M.; Vakili, M.H.; Ameri, E. Fabrication and evaluation of a biopolymer-based nanocomposite membrane for oily wastewater treatment. *Mater. Today Commun.* **2021**, *28*, 102560. [[CrossRef](#)]
31. Liang, S.X.; Jia, Z.; Zhang, W.C.; Li, X.; Wang, W.M.; Lin, H.C.; Zhang, L.C. Ultrafast activation efficiency of three peroxides by Fe₇₈Si₉B₁₃ metallic glass under photo-enhanced catalytic oxidation: A comparative study. *Appl. Catal. B Environ.* **2018**, *221*, 108–118. [[CrossRef](#)]
32. Zhang, C.; Wang, Y.; Zhang, X.; Guo, H. Fe₇₈Si₉B₁₃ amorphous alloys for the decolorization process of azo dye aqueous solutions with different initial concentrations at different reaction temperatures. *Vacuum* **2020**, *176*, 109301. [[CrossRef](#)]
33. Lai, B.; Zhang, Y.; Chen, Z.; Yang, P.; Zhou, Y.; Wang, J. Removal of p-nitrophenol (PNP) in aqueous solution by the micron-scale iron–copper (Fe/Cu) bimetallic particles. *Appl. Catal. B Environ.* **2014**, *144*, 816–830. [[CrossRef](#)]
34. Weng, C.-H.; Tao, H. Highly efficient persulfate oxidation process activated with Fe⁰ aggregate for decolorization of reactive azo dye Remazol Golden Yellow. *Arab. J. Chem.* **2018**, *11*, 1292–1300. [[CrossRef](#)]
35. Yamaguchi, R.; Kurosu, S.; Suzuki, M.; Kawase, Y. Hydroxyl radical generation by zero-valent iron/Cu (ZVI/Cu) bimetallic catalyst in wastewater treatment: Heterogeneous Fenton/Fenton-like reactions by Fenton reagents formed in-situ under oxic conditions. *Chem. Eng. J.* **2018**, *334*, 1537–1549. [[CrossRef](#)]

36. Xiong, Z.; Lai, B.; Yang, P.; Zhou, Y.; Wang, J.; Fang, S. Comparative study on the reactivity of Fe/Cu bimetallic particles and zero valent iron (ZVI) under different conditions of N₂, air or without aeration. *J. Hazard. Mater.* **2015**, *297*, 261–268. [[CrossRef](#)] [[PubMed](#)]
37. Chen, Q.; Yan, Z.C.; Zhang, H.; Kim, K.; Wang, W.M. Role of nanocrystallites of Al-based glasses and H₂O₂ in degradation azo dyes. *Materials* **2021**, *14*, 39. [[CrossRef](#)]
38. Qin, X.; Xu, J.; Zhu, Z.; Li, Z.; Fang, D.; Fu, H.; Zhang, S.; Zhang, H. Co₇₈Si₈B₁₄ metallic glass: A highly efficient and ultra-sustainable Fenton-like catalyst in degrading wastewater under universal pH conditions. *J. Mater. Sci. Technol.* **2022**, *113*, 105–116. [[CrossRef](#)]
39. Weber, E.J. Iron-Mediated Reductive Transformations: Investigation of Reaction Mechanism. *Environ. Sci. Technol.* **1996**, *30*, 716–719. [[CrossRef](#)]
40. SLiang, X.; Jia, Z.; Zhang, W.C.; Wang, W.M.; Zhang, L.C. Rapid malachite green degradation using Fe_{73.5}Si_{13.5}B₉Cu₁Nb₃ metallic glass for activation of persulfate under UV-vis light. *Mater. Des.* **2017**, *119*, 244–253.
41. Qin, X.D.; Li, Z.K.; Zhu, Z.W.; Fu, H.M.; Li, H.; Wang, A.M.; Zhang, H.W.; Zhang, H.F. Mechanism and kinetics of treatment of acid orange II by aged Fe-Si-B metallic glass powders. *J. Mater. Sci. Technol.* **2017**, *33*, 1147–1152. [[CrossRef](#)]
42. Zhu, S.; Xiang, Q.; Ma, C.; Ren, Y.; Qiu, K. Continuous electrocoagulation degradation of oily wastewater with Fe₇₈Si₉B₁₃ amorphous ribbons. *Environ. Sci. Pollut. Res.* **2020**, *27*, 40101–40108. [[CrossRef](#)] [[PubMed](#)]
43. Liang, C.; Guo, Y.-Y. Mass Transfer and Chemical Oxidation of Naphthalene Particles with Zerovalent Iron Activated Persulfate. *Environ. Sci. Technol.* **2010**, *44*, 8203–8208. [[CrossRef](#)] [[PubMed](#)]
44. Wang, L.; Yao, Y.; Zhang, Z.; Sun, L.; Lu, W.; Chen, W.; Chen, H. Activated carbon fibers as an excellent partner of Fenton catalyst for dyes decolorization by combination of adsorption and oxidation. *Chem. Eng. J.* **2014**, *251*, 348–354. [[CrossRef](#)]
45. Yurdakal, S.; Loddo, V.; Augugliaro, V.; Berber, H.; Palmisano, G. Photodegradation of pharmaceutical drugs in aqueous TiO₂ suspensions: Mechanism and kinetics. *Catal. Today* **2007**, *129*, 9–15. [[CrossRef](#)]
46. Huang, C.-M.; Pan, G.-T.; Li, Y.-C.M.; Li, M.-H.; Yang, T.C.-K. Crystalline phases and photocatalytic activities of hydrothermal synthesis Ag₃VO₄ and Ag₄V₂O₇ under visible light irradiation. *Appl. Catal. A Gen.* **2009**, *358*, 164–172. [[CrossRef](#)]
47. Ma, Y.; Rheingans, B.; Liu, F.; Mittemeijer, E.J. Isochronal crystallization kinetics of Fe₄₀Ni₄₀B₂₀ amorphous alloy. *J. Mater. Sci.* **2013**, *48*, 5596–5606. [[CrossRef](#)]
48. Niu, Y.; Bian, X.; Wang, W. Origin of ductile–brittle transition of amorphous Fe₇₈Si₉B₁₃ ribbon during low temperature annealing. *J. Non-Cryst. Solids* **2004**, *341*, 40–45. [[CrossRef](#)]
49. Mariano, N.; Souza, C.; May, J.; Kuri, S. Influence of Nb content on the corrosion resistance and saturation magnetic density of FeCuNbSiB alloys. *Mater. Sci. Eng. A* **2003**, *354*, 1–5. [[CrossRef](#)]
50. Lin, B.; Bian, X.; Wang, P.; Luo, G. Application of Fe-based metallic glasses in wastewater treatment. *Mater. Sci. Eng. B* **2012**, *177*, 92–95. [[CrossRef](#)]